Surface Science 606 (2012) 12–20

Contents lists available at SciVerse ScienceDirect

Surface Science

journal homepage: www.elsevier.com/ locate/susc

Modeling ammonia oxidation over a Pt (533) surface

Matías Rafti [a,b,*], José Luis Vicente [b], Alberto Albesa [b], Axel Scheibe [a], Ronald Imbihl [a]

[a] Institut für Physikalische Chemie und Elektrochemie, Leibniz-Universität Hannover, Callinstr. 3-3a, 30167 Hannover, Germany
[b] Instituto de Investigaciones Fisicoquímicas Teóricas y Aplicadas (INIFTA), Dpto. de Química, Universidad Nacional de La Plata, Diag 113 y 64 cc. 16 suc. 4 (1900) La Plata, Argentina

ARTICLE INFO

Article history:
Received 7 March 2011
Accepted 22 August 2011
Available online 27 August 2011

Keywords:
Computer simulations
Models of surface kinetics
Catalysis
Adsorption kinetics
Surface chemical reaction
Platinum
Ammonia
Single crystal surfaces

ABSTRACT

We present a new reaction model for ammonia oxidation on a Pt (533) surface and perform numerical simulations using mean field equations. Kinetic parameters were taken from experiments and Density Functional Theory (DFT) calculations. The model is based on an oxygen-activated ammonia decomposition and includes NHx (x = 0, 1, 2) intermediates. Reaction rates and coverages obtained from calculations show semiquantitative agreement with values from kinetic and in-situ XPS measurements up to 0.1 mbar pressures. Pathways for ammonia oxidation were analyzed by varying kinetic parameters in the model, which provides new insights into the relative importance of different reaction steps.

1. Introduction

The selective oxidation of ammonia with air over Pt/Rh catalysts to NO in the so-called Ostwald process is one of the most important catalytic processes in chemical industry. In environmental catalysis the oxidation of ammonia to nitrogen is a key step in removing air pollutants in the so-called selective catalytic reduction (SCR) process [1]. With regard to the significance of catalytic ammonia oxidation it is quite surprising that relatively few mechanistic and kinetic studies have been performed. The lack of interest in a precise modeling of ammonia oxidation can be traced back to the fact that under the conditions of the Ostwald process (T>900 K) the production of NO is limited by mass transport to the surface and not by surface processes. Over the past ten years a number of microkinetic models have been proposed which all rely on the assumption that ammonia decomposition on platinum is activated through direct interaction of ammonia with chemisorbed oxygen or OH species, whereas non-activated decomposition of ammonia plays a negligible role [2–6]. These models are all quite similar and they all succeed in reproducing the main qualitative features of the experiment. What is missing in these simulations is a detailed comparison with experimental data, in particular, with respect to a quantification of adsorbate coverages and with respect to the structure sensitivity of the reaction. Providing such a detailed comparison is the aim of this paper.

Single crystal studies of ammonia oxidation have been conducted with Pt (100), Pt (111) and with various stepped and kinked Pt (111) surfaces [7–15]. Most of these studies were performed at low pressure, in the range from 10^{-9} to 10^{-4} mbar. In an attempt to bridge the so-called pressure gap, the reaction studies were extended up to 0.1 mbar for various orientations [16,17]. To circumvent heat and mass transport problems, investigations with supported Pt and with monolithic polycrystalline Pt were conducted in microreactors [18].

On the theoretical side ammonia decomposition and the interaction of ammonia with oxygen was studied with DFT (density functional theory) calculations for Pt (111), Pt (100), and Pt (211) [19–23]. Both, the experimental as well as the theoretical studies agree that ammonia decomposition is activated by adsorbed oxygen or OH. The alternative pathway of first decomposing ammonia on a bare Pt surface followed by recombination of the fragments with oxygen and OH, plays a negligible role under typical experimental conditions.

Possible products in ammonia oxidation are N_2, NO, N_2O, and H_2O as reflected by the following reaction equations:

$$4NH_3 + 5O_2 \rightarrow 4NO + 6H_2O$$
$$4NH_3 + 3O_2 \rightarrow 2N_2 + 6H_2O$$
$$4NH_3 + 4O_2 \rightarrow 2NO_2 + 6H_2O$$

* Corresponding author at: Instituto de Investigaciones Fisicoquímicas Teóricas y Aplicadas (INIFTA), Dpto. de Química, Universidad Nacional de La Plata, Diag 113 y 64 cc. 16 suc. 4 (1900) La Plata, Argentina.
E-mail address: mrafti@quimica.unlp.edu.ar (M. Rafti).

0039-6028/$ – see front matter © 2011 Elsevier B.V. All rights reserved.
doi:10.1016/j.susc.2011.08.014

The availability of oxygen controls the competition between N_2 vs. NO formation. A large O_2/NH_3 ratio and a high temperature favour NO formation, whereas at low temperatures and low O_2/NH_3 ratios N_2 is the preferred reaction channel. N_2O is a byproduct which is formed in significant amounts only at higher pressure ($>10^{-2}$ mbar). Due the disastrous effect on global warming, N_2O formation is an undesired byproduct.

Experiments in which Ar and He were added as inert gas showed that at p = 30–60 mbar and T = 523 K mass transport limitations become significant above 660 K [7]. Unless a model takes explicitly mass and heat transport into account, which means solving the Navier–Stokes equations for the reactor, a simulation is meaningful only up to 10^{-1} mbar. A full reactor model was used by Rebrov et al. [24,25] to simulate ammonia oxidation over Pt/Al_2O_3 in microreactor at pressures close to 1 bar. Scheibe et al. [2] formulated a model specifically aimed at describing ammonia oxidation over the stepped Pt single crystal surfaces, Pt (533) and Pt (433). Kraehnert and Baerns [18] in their model, simulated ammonia oxidation over a Pt foil in a microstructured reactor at pressures $<6\times10^{-2}$ mbar. All these models are rather similar in the sense that oxygen activates ammonia decomposition. The oxygen-activated decomposition is lumped into one step while NHx (x = 1, 2) intermediates as well as hypothetical oxygen containing NHxOy intermediates are not considered.

The reason to neglect decomposition intermediates was that the corresponding kinetic parameters were not available at that time. Only when DFT calculations yielded reaction profiles for the complete pathways of OH- and O-assisted ammonia decomposition in Pt (111), Pt (100) and Pt (211), the missing kinetic constants became accessible. With in situ XPS, the adsorbate coverages during ammonia oxidation over Pt (533) have been followed at two different pressure ranges, 10^{-4} mbar and at 10^{-1} mbar [17].

In this study we chose Pt (533) as model system because, in addition to the XPS experiments, kinetics of ammonia oxidation have been studied over a vast pressure range from 10^{-6} to 10^{-2} mbar [26,27]. Stepped Pt (111) surfaces can be considered as model system for a real, that is polycristalline, Pt catalyst. A flat Pt (111) surface is not a good model system because (due to a low O_2 sticking probability) will exhibit low catalytic activity [28]. The unreconstructed Pt (100) surface exhibits also a high catalytic activity but compared to stepped Pt (111) surfaces, this orientation has the additional complication of an adsorbate-induced surface reconstruction [29,30].

The main motivation to study the kinetics of ammonia oxidation on Pt (533) over a vast pressure range was to bridge the so-called pressure gap in heterogeneous catalysis. The Ostwald process is conducted at atmospheric pressure. At elevated pressures an oxidation of the Pt catalyst might take place, but up to nearly 1 mbar no signs of any oxide formation were found in XPS [17]. Another complication is the reaction-induced restructuring of the Pt catalyst [31,32]. In the Ostwald process, the Pt/Rh gauze becomes visibly roughened already during the first minutes of operation. The extent of reaction-induced restructuring is dependent on the total pressure but also under the mild conditions of an experiment in an UHV environment the Pt surface is modified by the reaction. On Pt (533) at pressures beyond 1×10^{-4} mbar a reversible doubling of the step height occurred under certain reaction conditions [22,26]. Since the effect is pressure dependent, reaction-induced restructuring is part of the pressure as well of the material gap.

In the simulations here presented, the catalyst was treated as rigid surface; that is, we neglect dynamic restructuring effects caused by the surface reaction. As will be shown, with this approach we achieve a semi-quantitative modeling of the kinetics. The results provide us with insights into the pathways of ammonia oxidation, essentially confirming the importance of the oxygen activated ammonia decomposition.

2. The model

2.1. The reaction mechanism and mathematical equations

The model describes the reaction under isothermal conditions with heat and mass transport limitations playing no role. The conversion rate is assumed to be small so that readsorption of products is negligible. The surface is considered as rigid, i.e. reaction-induced restructuring effects do not exist.

The Pt (533) surface also written as 4 (111) × (100) consists of 4 lattice units wide (111) terraces, separated from each other by a step with (100) orientation, as demonstrated by the structural model of Pt (533) in Fig. 1. Since at least two reaction steps, O_2 adsorption and NO decomposition are known to be highly structure sensitive, the question is how to describe the behavior of the Pt (533) surface which is composed of (100) and (111) facets. NO-decomposition/NO-formation should be restricted to the (100) step sites, whereas the (111) terrace sites should be fairly inactive [33–36]. In the model, we do not formulate separate equations for the step and for the terrace sites but we homogenize the surface. Through the choice of the constants we can, however, take into account that the (100) steps govern the catalytic activity of Pt (533) for certain reaction steps. The various adsorbates occupy different adsorption sites on Pt (100) and Pt (111) but in the model we assume a single adsorption site. So-called dual-adsorption sites models have been proposed [24]; the underlying assumption of two adsorption sites which can be populated completely independent of each other is, however, unphysical because energetic interactions or site blocking by steric effects will in any case cause dependence [37].

Transforming the set reaction equations R1–R13a into kinetic equations, we arrive to a set of 7th-order coupled ordinary differential equations (ODE's) plus one independent expression for the amount of free sites. Eqs. (1)–(8) describe the variation of the surface coverages of O, OH, NHx, (x = 0–3), NO, and vacant sites (symbolized as * with coverage θ_*):

$$O_2(g) + 2* \underset{k2}{\overset{k_1}{\leftrightarrow}} 2O_{ad} \quad [R1]$$

$$NH_3(g) + * \underset{k_4}{\overset{k_3}{\leftrightarrow}} NH_{3,ad} \quad [R2]$$

$$NH_{3,ad} + O_{ad} \underset{k_6}{\overset{k_5}{\leftrightarrow}} NH_{2,ad} + OH_{ad} \quad [R3]$$

$$NH_{2,ad} + O_{ad} \underset{k_8}{\overset{k_7}{\leftrightarrow}} NH_{2,ad} + OH_{ad} \quad [R4]$$

$$NH_{ad} + O_{ad} \underset{k_{10}}{\overset{k_9}{\leftrightarrow}} N_{ad} + OH_{ad} \quad [R5]$$

$$NH_{3,ad} + OH_{ad} \overset{k_{11}}{\rightarrow} NH_{2,ad} + H_2O(g) + * \quad [R6]$$

$$NH_{2,ad} + OH_{ad} \overset{k_{12}}{\rightarrow} NH_{ad} + H_2O(g) + * \quad [R7]$$

$$NH_{ad} + OH_{ad} \overset{k_{13}}{\rightarrow} N_{ad} + H_2O(g) + * \quad [R8]$$

$$2OH_{ad} \overset{k_{14}}{\rightarrow} O_{ad} + H_2O(g) + * \quad [R9]$$

$$2N_{ad} \overset{k_{15}}{\rightarrow} N_2(g) + 2* \quad [R10]$$

$$N_{ad} + O_{ad} \underset{k_{17}}{\overset{k_{16}}{\leftrightarrow}} NO_{ad} + * \quad [R11]$$

$$NO_{ad} \overset{k_{18}}{\rightarrow} NO(g) + * \quad [R12]$$

$$NO_{ad} + N_{ad} \overset{k_{19}}{\rightarrow} N_2O(g) + 2* \quad [R13a]$$

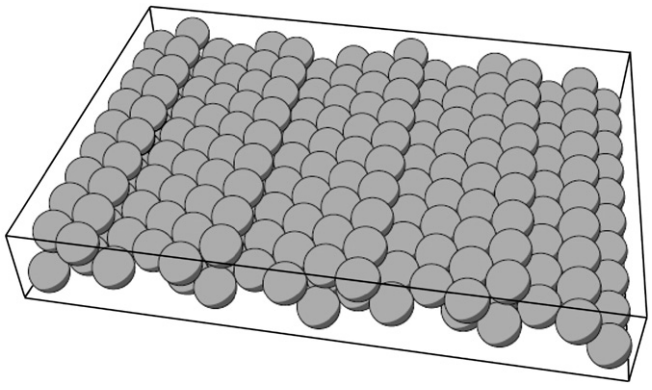

Fig. 1. Ball model of the Pt (533) surface.

$$\frac{d\theta_o}{dt} = \left\{ \begin{array}{l} 2k_1 p_{o2}\theta_*^2 + 2\theta_h k_1 p_{o2}(1-2.5\theta_o)^2 - 2k_2\theta_o^2 - k_5\theta_{NH3}\theta_o + k_6\theta_{NH2}\theta_{OH} \cdots \\ -k_7\theta_{NH2}\theta_o + k_8\theta_{NH}\theta_{OH} - k_9\theta_{NH}\theta_O + k_{10}\theta_N\theta_{OH} + k_{14}\theta_{OH}^2 - k_{16}\theta_o\theta_N \cdots \\ +k_{17}\theta_{NO}\theta_* \end{array} \right\} \quad (1)$$

$$\frac{d\theta_{NH3}}{dt} = k_3 p_{NH3}\theta_* - k_4\theta_{NH3} - k_5\theta_{NH3}\theta_o + k_6\theta_{NH2}\theta_{OH} - k_{11}\theta_{NH3}\theta_{OH} \quad (2)$$

$$\frac{d\theta_{NH2}}{dt} = \left\{ \begin{array}{l} k_5\theta_{NH3}\theta_o - k_6\theta_{NH2}\theta_{OH} - k_7\theta_{NH}\theta_o + k_8\theta_{NH}\theta_{OH} + k_{11}\theta_{NH3}\theta_{OH} \cdots \\ -k_{12}\theta_{NH2}\theta_{OH} \end{array} \right\} \quad (3)$$

$$\frac{d\theta_{NH}}{dt} = \left\{ \begin{array}{l} k_7\theta_{NH2}\theta_o - k_8\theta_{NH}\theta_{OH} - k_9\theta_{NH}\theta_o + k_{10}\theta_N\theta_{OH} + k_{12}\theta_{NH2}\theta_{OH} \cdots \\ -k_{13}\theta_{NH}\theta_{OH} \end{array} \right\} \quad (4)$$

$$\frac{d\theta_{OH}}{dt} = \left\{ \begin{array}{l} k_5\theta_{NH3}\theta_o - k_6\theta_{NH2}\theta_{OH} + k_7\theta_{NH2}\theta_o - k_8\theta_{NH}\theta_{OH} + k_9\theta_{NH}\theta_o \cdots \\ -k_{10}\theta_N\theta_{OH} - k_{11}\theta_{NH3}\theta_{OH} - k_{12}\theta_{NH2}\theta_{OH} - k_{13}\theta_{NH}\theta_{OH} - 2k_{14}\theta_{OH}^2 \end{array} \right\} \quad (5)$$

$$\frac{d\theta_N}{dt} = \left\{ \begin{array}{l} k_9\theta_{NH}\theta_o - k_{10}\theta_N\theta_{OH} + k_{13}\theta_{NH}\theta_{OH} - 2k_{15}\theta_N^2 - k_{16}\theta_o\theta_N \cdots \\ +k_{17}\theta_{NO}\theta_* - k_{19}\theta_N\theta_{NO} \end{array} \right\} \quad (6)$$

$$\frac{d\theta_{NO}}{dt} = k_{16}\theta_o\theta_N - k_{17}\theta_{NO}\theta_* - k_{18}\theta_{NO} - k_{19}\theta_{NO}\theta_N \quad (7)$$

$$\theta_* = 1 - 2.5(\theta_o + \theta_{NH3} + \theta_{NH2} + \theta_{NH} + \theta_{OH} + \theta_N) - 1.6\theta_{NO} \quad (8)$$

The values for the constants are summarized in Table 1, while the temperature independent constants are shown in Table 2. The initial sticking coefficients for the gases ($s_{0,i}$, with i = 1, 3 for O_2 and NH_3 respectively) contained in k_1 and k_3, are connected to the impingement rates of gas particles, λ_i (i = 1, 3) via $k_i = \lambda_i s_{0,i}$.

$$\lambda_i \frac{1}{\sqrt{2\pi m_i k_B T}} \quad (9)$$

For the adsorption and desorption parameters of the gases we rely on experimental values. Prefactors in the expression for the vacant sites were derived from the estimated saturation coverages of the adsorbates. Only for Pt (533)/O the saturation coverage has been determined as 0.25 ML for the (111) terraces and 0.12 ML for the step sites, giving altogether $\theta_{sat,O} = 0.25 + 0.12 \approx 0.4$ [38,39]. The same saturation coverage was assumed for all adsorbates occupying fcc sites on Pt (111). For Pt (111)/NH_3, a saturation coverage of 0.25 has been determined for the α-state [21,40]. With exception of NO, the same saturation coverage was taken for all adsorbates occupying bridge or on top sites on Pt (111); i.e., NH_3, NH_2, and OH. For NO the situation is different because the vacant sites not only control NO adsorption but also NO decomposition ($R11^{-1}$). On Pt (100) NO dissociation was shown to be inhibited beyond a coverage of 0.6 ML [41]. Accordingly, a prefactor of 1.6 was taken for NO coverage since we assume that only the (100) sites on Pt (533) are active in NO dissociation.

Before DFT calculations with ammonia oxidation on Pt surfaces were started, all kinetic constants involving surface intermediates were unknown. With DFT, reaction profiles have been calculated for Pt (111), Pt (211), and Pt (100). For stepped surfaces, a large number of possible pathways exists and therefore for Pt (211) only a selection of the most plausible reaction pathways has been computed [3,7,19].

Table 1
Kinetic parameters used in the simulations. Unless otherwise specified, rate constants were calculated assuming an Arrhenius-type temperature dependence ($k_i = \nu_i \exp[-E_i/k_B T]$).

Step	Constant	E_i (kJ mol^{-1})	ν_i (s^{-1})	Ref.
R1[a]	k_1	−12	s.text	[39]
$R1^{-1}$	k_2	185	3.6×10^{13}	[2]
R2 [a]	k_3	s.text	s.text	[2]
$R2^{-1}$	k_4	69	2.0×10^{10}	[19] + fit
R3	k_5	55	3.7×10^{11}	[7]
$R3^{-1}$	k_6	22	3.0×10^{11}	[7]
R4	k_7	87	6.1×10^{12}	[7]
$R4^{-1}$	k_8	128	3.0×10^{11}	[7]
R5	k_9	84	1.0×10^{13}	[7] + fit
$R5^{-1}$	k_{10}	57	3.0×10^{11}	[7] + fit
R6	k_{11}	73	3.9×10^{12}	[20]
R7	k_{12}	22	3.4×10^{12}	[20]
R8	k_{13}	22	5.1×10^{11}	[20]
R9	k_{14}	75	1.0×10^{13}	[42]
R10	k_{15}	100	2.0×10^{11}	[2] + fit
R11	k_{16}	85	2.0×10^{15}	[41] + fit
$R11^{-1}$	k_{17}	100	2.0×10^{15}	[41]
R12	k_{18}	163	8.0×10^{14}	[2]
R13a	k_{19}	155	1.1×10^{14}	[18] + fit

[a] No simple Arrhenius expression used, see text.

Table 2
Temperature independent constants used in the simulations.

Constant	Description	Value	Ref.
α	O_2 stick. prob. into precursor state	0.33	[39]
ν_d/ν_c	O_2 freq. factor ratio into precursor state	18	[39]
$s_{0,3}$	NH_3 initial sticking coef.	0.47	[26]
$\theta_{sat,O}$	Oxygen sat. coverage	0.4	[38],[39]
$\theta_{sat,NO}$	NO sat. coverage	0.6	[41]
θ_h	Surface defect sites	0.0001	*this work*

2.2. Adsorption and desorption

Oxygen adsorbs dissociatively on Pt and therefore two adjacent vacant sites are required, leading to a square dependence on the number of vacant sites (θ_*). We also assume that certain fraction of defect sites, θ_h, are present on the surface which cannot be blocked for oxygen adsorption by other adsorbates. As guidelines for the correct choice of sticking coefficients, we can use the experimentally measured reactive sticking coefficients for O_2 and NH_3, which represent a lower limit for the values [26]. Ammonia adsorption can be considered as moderately structure sensitive since the initial sticking coefficient was shown to vary about one order of magnitude from NH_3 adsorption on Pt (111) to adsorption on Pt (210) [23]. For Pt (533)/NH_3 a value of 0.47 was taken for $s_{0,3}$[26].

On stepped Pt (111) surfaces the sticking coefficient for O_2 increases with the step density and it decreases with rising temperature [38,39,43]. The decrease with temperature, which formally corresponds to negative activation energy, is due to the fact that dissociation occurs via a molecular precursor state, which becomes less populated with increasing temperature. Oxygen adsorption on Pt (533) has been studied by Gee and Hayden [39] with a molecular beam. In a temperature range from 100–655 K they fitted the temperature dependence of the initial sticking coefficient for oxygen, $s_{0,1}$, with a precursor model for oxygen,

$$s_{0,1} = \alpha\left[\frac{\nu_d}{\nu_c}\exp\left(-\frac{E_1}{RT}\right) + 1\right]^{-1} \quad (10)$$

with α denoting the sticking probability into the precursor state, ν_d and ν_c being the frequency factors for desorption from this molecular state and transition into the dissociated state, respectively, and E_1 is the corresponding difference in activation energy. As in preceding simulations we used the values of Gee and Hayden with exception of the ratio $\nu_d/\nu_c = 18$, instead of 80 [2]. This accounts for the fact that our gas temperature of 300 K corresponds only to 25 meV, in contrast to the 52 meV for which the parameters were originally

fitted. For α, a value of 0.33 was used. Simple Langmuirian adsorption kinetics was assumed for both gases, O_2 and NH_3.

2.3. Ammonia decomposition

With DFT, energy profiles have been calculated for Pt (111), Pt (100), and Pt (211) comparing ammonia decomposition on a bare Pt surface with decomposition activated by chemisorbed oxygen, O and by OH adspecies [19]. The DFT calculations for Pt(100) by Novell-Leruth et al. [3] showed that similar to Pt(111), the barriers for the decomposition of pure ammonia are about 30–80 kJ mol^{-1} higher than the barriers for oxygen-activated decomposition. As demonstrated for Pt (111), both adsorbed O and OH reduce the activation barriers for stepwise ammonia decomposition, but while O-species just reduces strongly the barrier for the first step R3, OH also activates all subsequent decomposition steps. On Pt(100) the favorable role of OH compared to O does not hold because on this surface the latter reduces the barriers to a bigger extent. From a comparison of Pt(111) with the stepped surface Pt(211), it was concluded that with exception of the removal of the last proton, steps do not promote oxygen-activated ammonia decomposition [7].

Consequently, in the simulation we first tried to incorporate the activation barriers and frequency factors calculated for Pt(111). Since the barrier for the O-assisted NH decomposition is quite high the surface becomes easily poisoned by a large NH coverage. Comparing Pt (211) with Pt (111), it has been concluded that steps substantially reduce the activation barrier for the NH + O reaction. Accordingly, a value of 52 kJ mol^{-1} for this step was initially used for the simulation, as suggested in ref. [19]. The simulations then showed that this value had to be modified to 84 kJ mol^{-1} (s. below).

2.4. NO formation/decomposition

Experimentally, NO dissociation on Pt was shown to be extremely structure sensitive. In TPD (temperature programmed desorption) of adsorbed NO the smallest activity is shown by Pt (111) where less than 10% decompose during desorption, while about 60% decompose on Pt (100), and 90% on Pt (410) [35]. Similar to Pt (100), adsorbed NO on Pt (533) starts to dissociate beyond T = 400 K [44]. As a consequence of the vacant site requirement for NO dissociation (step $R11^{-1}$), large adsorbate coverages on Pt (100) were shown to inhibit NO dissociation. The autocatalytic proliferation of the vacant sites which follows from the inhibition effect of coadsorbates was shown to be the main driving force for the rate oscillations and chemical waves in NO reducing reactions on Pt (100) [41]. The activation barrier for NO decomposition on Pt (100) was experimentally determined to be 103 kJ mol^{-1}[41], but for the reverse step of NO formation, no corresponding experimental value is available.

The adsorption of NO and the decomposition of NO and recombination of the fragments were investigated via DFT calculations by Offermans et al. for Pt (111) and Pt (211) [16,20] and by Bogicevic and Hass [45]; and for Pt (100) surfaces by Novell–Leruth et al. [3] and Ge and Neurock [46]. As expected, for the inactive Pt (111) surface the barriers for NO dissociation were quite high with 203 kJ mol^{-1} and 237 kJ mol^{-1}, respectively. On Pt (100) Novel-Leruth et al. found an activation energy of 88 kJ mol^{-1} which is not very far from the experimental value. The reverse step, the recombination of N and O adsorbed into NO adsepcies was only weakly activated on Pt (100) with 11 kJ mol^{-1} according to their calculations. Ge and Neurock studied the structure dependence of NO decomposition conducting DFT calculations for Pt (100)–(1 × 1), Pt (211), and Pt (410). They found that not all steps but only those with (100) orientation promotes NO dissociation. Their value of 93 kJ mol^{-1} proposed for Pt (100) surface is not far from the value of Novell–Leruth et al. For Pt (533) a surprisingly high value for NO decomposition was calculated by Backus et al. with Ea = 157 kJ mol^{-1}[44].

2.5. H_2O formation

Water formation on Pt (111) has been studied in modulated molecular beam experiments and later on, at low temperature, with scanning tunneling microscopy [42,47]. In DFT calculations aimed at reproducing the STM results Michaelides et al. [48] found that the formation of an OH adspecies from H and O is, with Ea = 100 kJ mol^{-1}, a strongly activated process whereas the addition of the second proton with Ea = 19 kJ mol^{-1} exhibits only a small barrier. These values do not all agree at all with the experimentally determined barriers in ref. [42].

In the reaction scheme applied in this work, ammonia decomposition without oxygen activation is neglected and, consequently, no adsorbed hydrogen is generated. For this reason H_2O formation can only occur through OH disproportionation as described in step R9 and through H abstraction from NHx, (x = 1–3) by adsorbed OH in steps R6–R8. The activation barrier for OH disproportionation on Pt (111) was calculated to be 13 kJ mol^{-1} which is far from the experimentally determined value of 80 kJ mol^{-1}. The large deviation might be due to the fact that the calculation was conducted for an ordered low temperature coadsorption phase. For our simulation the experimentally determined value was taken.

2.6. N_2O formation

N_2O in ammonia oxidation is formed in larger quantities only at high pressure (> 10^{-2} mbar). In NO reducing reactions such as hydrogen reduction on Pt (100), N_2O is formed also at pressures as low as 10^{-6} mbar [41]. In TPD of adsorbed NO on Pt (533) small amounts of N_2O were detected [44]. For the formation of N_2O two main reaction pathways can be formulated, firstly by the recombination of adsorbed nitrogen with NO as described by step R13a, or via dimerization of adsorbed NO via step R13b,

$$2NO_{ad} + (NO)_{2,ad} \rightarrow N_2O(g) + O_{ad} + * \quad [R13b]$$

In addition, also the reaction of NO with an hydrogen containing N-species, NHx, (x = 1–3), to N_2O has been considered. Experimentally, the formation of N_2O in the $NH_3 + O_2$ reaction over Pt and N_2O decomposition, has been studied with a TAP (Transient Analysis of Products) reactor in a pressure range from 10^{-6}–10^{-1} mbar, at temperatures between 373 and 1073 K [16,18]. Since a dimerization of adsorbed NO has been observed on a number of metal surfaces, the bimolecular reaction pathway to N_2O formation on Pt (111) via step R13b was investigated with DFT by Bogicevic and Hass [45]. Their conclusion was that the bimolecular pathway is rather unlikely on a flat Pt (111) surface but that steps might promote this reaction pathway. For the N + NO route in step R13a, Novell-Leruth et al. calculated a relatively low activation barrier of 69 kJ mol^{-1} for Pt (100). In our simulations the bimolecular pathway R13b yielded results far off the experiment and therefore only pathway R13a was considered.

3. Results and discussion

3.1. Temperature programmed desorption and stationary kinetics

In order to test the ability of the proposed model to reproduce the experimental behaviour, simulations of Temperature Programmed Desorption (TPD) of NO on a Pt (533) surface were carried using different initial NO coverages. Good agreement with experimental TPD profiles as reported by Backus et al. [44] was reached; i.e., low initial coverages (θ_{NO}) were observed to favour NO dissociation (and thus N_2 and N_2O formation), while using increasingly higher θ_{NO} values causes an increase of initial NO desorption. In good agreement with experiments also, simulations results show that N_2O formation remains below 1% of the N_2 and NO obtained values; temperatures

obtained for NO dissociation start and maximum desorption rate are ≈50 K higher than experimental values reported in ref. [44], which is an acceptable level of agreement given the uncertainty of model parameters used.

The proposed model was also compared to experimental results obtained for ammonia oxidation over Pt (533) in a pressure range from 10^{-5} to 10^{-2} mbar [26,27], Fig. 2 displays simulated and measured temperature profiles of the stationary reaction rates for three different ratios O_2/NH_3 in the 10^{-4} mbar range. Shown are the two main products, N_2 and NO, for $p_{O2} : p_{NH3} = 1 : 1$, for oxygen being in excess with a 3 : 1 ratio and for oxygen in large excess with a 10 : 1 ratio of the reactants. With regard to the fact that the absolute reaction rates in the experiment are probably only accurate within a factor of 1.5, the agreement between experimental and simulated rate curves is quite good. The overall behavior of N_2 formation being the dominant pathway at low temperature and NO prevailing at high temperature is determined mainly by the availability of oxygen and by the kinetic parameters controlling NO formation and desorption (k_{16}, k_{17}, k_{18}).

With increasing O_2/NH_3 ratio, the maxima in the measured N_2 and NO production curves shift to lower temperature by roughly 50–100 K. In the simulated NO curves this trend is reproduced, but in the calculated N_2 rate traces, the shift is strongly reduced from a rate maximum at 620 K at 1 : 1 ratio to 580 K at 10 : 1 ratio. Increasing the total pressure by about two orders of magnitude to 10^{-2} mbar, leads to the rate traces reproduced in Fig. 3 for a $p_{O2} : p_{NH3} = 1 : 1$ ratio of the reactants. With respect to the 10^{-4} mbar data, the rate maxima underwent a considerable shift to higher temperature from 620 K to 755 K for N_2 production. As demonstrated by Fig. 4 a), the simulation reproduces quite well the experimentally observed shift of the N_2 rate maximum temperature with total pressure increase. In the pressure range from 10^{-5} mbar to 10^{-1} mbar, the maximum in N_2 production scales with the total pressure as demonstrated by Fig. 4 b). The experimental data show this scaling only up to 10^{-3} mbar. Whether the strong restructuring that is observed in LEED at, and beyond 10^{-3} mbar is responsible for the deviation from linear scaling, remains to be shown. Since the experimental data were obtained with different reactors, inaccuracies in the determination of the absolute reaction rates might also cause a change in the slope.

Reversible restructuring of the surface involving a doubling of the atomic step height, was shown to cause broad hysteresis in experiments [26]. In this work the surface is treated as rigid, and consequently no multistability occurs in the simulated rate curves.

3.2. Adsorbate coverages

In situ measurements with differentially pumped XPS allows to follow adsorbate coverages during ammonia oxidation over Pt (533) up to a relatively high pressure, 10^{-1} mbar [17]. A comparison of measured and calculated adsorbate coverages is displayed in Fig. 5. The main role played by oxygen coverage (θ_O) when analyzing the preferred reaction pathway of ammonia oxidation was discussed in several studies [7–11], high (low) θ_O switches selectivity towards NO (N_2) production, and therefore accurate modeling should address this point. Oxygen coverages obtained from simulations (dark blue areas in Fig. 5) successfully reproduced the experimentally observed trends, i.e., for increasingly higher pressures, higher θ_O limit is reached in T-evolution coverage plots. Namely, in the 10^{-4} mbar range, $\theta_O \approx 0.01$ ML simulations and experimental limit only builds up beyond 500 K; with O_2:NH_3 ratio of 10 : 1, the $\theta_O \approx 0.025$ ML experimental limit value is comparable to $\theta_O \approx 0.04$ ML obtained from

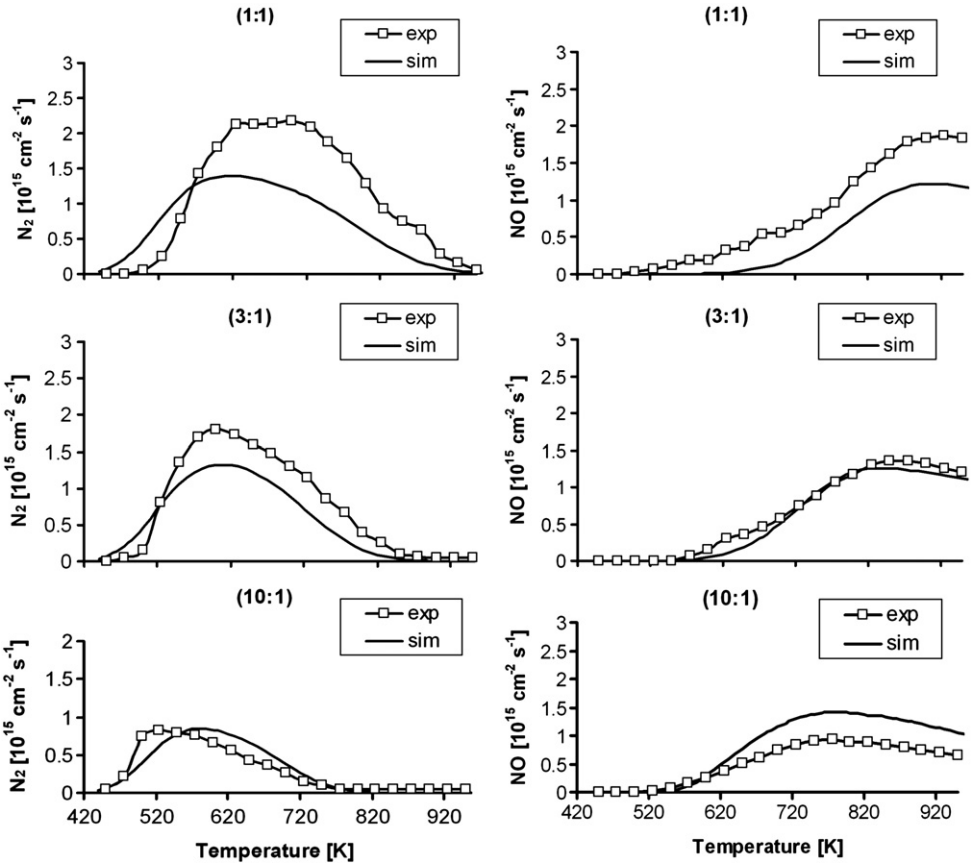

Fig. 2. Comparison between simulated and experimental temperature profiles of the reaction in the 10^{-2} mbar range. Shown are the stationary N_2 (left panel) and NO (right panel) production rates for varying ratios $p_{O2} : p_{NH3}$ as indicated in every plot, keeping $p_{O2} = 1 \times 10^{-4}$ mbar for all the simulations. Experimental data from ref. [26]).

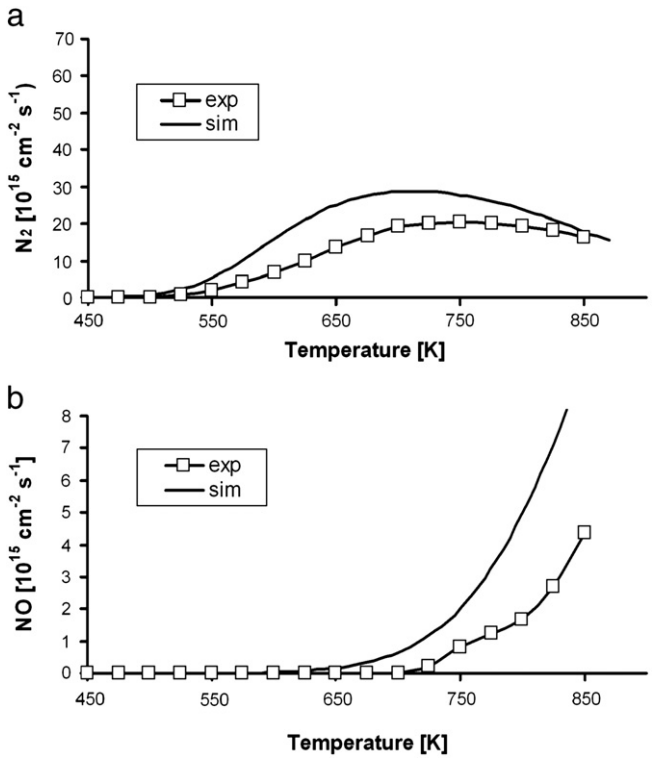

Fig. 3. Comparison between simulated and experimental temperature profiles of the reaction in the 1×10^{-2} mbar range. (a) N_2 production (b) NO production. Reaction conditions: $p_{O2} : p_{NH3} = 1 : 1$; ptot $= 1\times10^{-2}$ mbar. Experimental data from ref. [27].

Despite the above discussed well-reproduced features, striking differences can be noted between calculated and XPS measured coverages in Fig. 5. In order to rationalize such differences, one has to consider a number of facts inherent to the experiments analyzed. In XPS data, additional species appear, such as a carbon (C, yellow area reactively removed at high temperatures), carbon containing N contamination (N_C, light grey), and (due to the presence of silicon in the high pressure cell in the experiments which causes SiO_2 accumulation on the surface) an additional oxygen signal denoted as O_{OX} (light blue in Fig. 5) which presumably just blocks a certain fraction of the catalytic surface. Surprisingly, no NO was detected on XPS experiments while simulation show some non-zero θ_{NO} for T<650 K. Photon induced desorption or decomposition could play a role, but adsorption measurements demonstrated that this species decomposes easily on Pt (533). Only a small fraction of the originally adsorbed NO at T = 300 K remained intact when the sample was heated at T = 375 K. Fast thermal decomposition is therefore the most likely explanations for the absence of NO in the XPS experimental results.

3.3. Reaction pathways and influence of kinetic parameters

In the experiments with Pt (533), no N_2O was detected, but this does not rule out that a small amount (<5%) is produced, since without the use of isotopically labelled NH_3 the signals of CO_2 and N_2O overlap in mass spectra. For comparison with experiment, data reported by Baerns et al. [16,18], who studied ammonia oxidation over a Pt foil at atmospheric pressure in a microreactor can be used. Relative to the maximum in N_2 production, about 5% of N_2O were generated in temperature range extending roughly from 700 to 850 K. In the simulation, the experimentally observed tendency that

simulations. For the higher pressure range explored 10^{-1} mbar, chemisorbed oxygen is always present on the surface reaching 0.24 ML in the experiment, while simulations performed show a comparable value of 0.14 ML. The oxygen coverage exhibits a relative minimum when the N_2 production rate is at maximum, both in simulations and experimental results. Because of the small separation of the N *1 s* signals it was not possible in the XPS experiments to distinguish between NH and NH_2 adsorbates. Both species are therefore summarized under NHx (x = 1, 2). In the experiment, the N containing species decrease strongly beyond 400–500 K leading to a nearly N-free surface in the 10^{-4} mbar pressure regime above 700 K, and in the 10^{-1} mbar range above 800 K. This trend is well reproduced in the simulations.

In the simulations, coverages of NH and NH_2 species (not showed here) were found to vary in parallel, thus indicating that both are in chemical equilibrium. The θ_{NH} observed value is slightly higher than θ_{NH2} which is to be expected from the higher thermodynamic stability of NH compared to NH_2. The OH-activated pathways of ammonia decomposition play a very minor role despite the favourable activation barriers; this can be attributed to the low coverages observed.

Qualitatively, the same species are seen in the simulations and in the experiment but larger differences are observed in the quantitative distribution. At 10^{-4} mbar and 3 : 1 ratio of reactants, the different ad-species N, NHx, and NH_3 have about equal weight in the experiment at low temperature; whereas ammonia exhibits a very small coverage in the simulation. Increasing the oxygen content to a 10 : 1 ratio naturally enhances the formation of the final ammonia decomposition product (N) in the simulation. In the experiment this also seen, but the NHx (x = 1, 2) intermediates strongly grow instead. Evidently, a substantial activation barrier prevents removal of the last proton (step R5 of the proposed mechanism). This barrier is too low in the simulation.

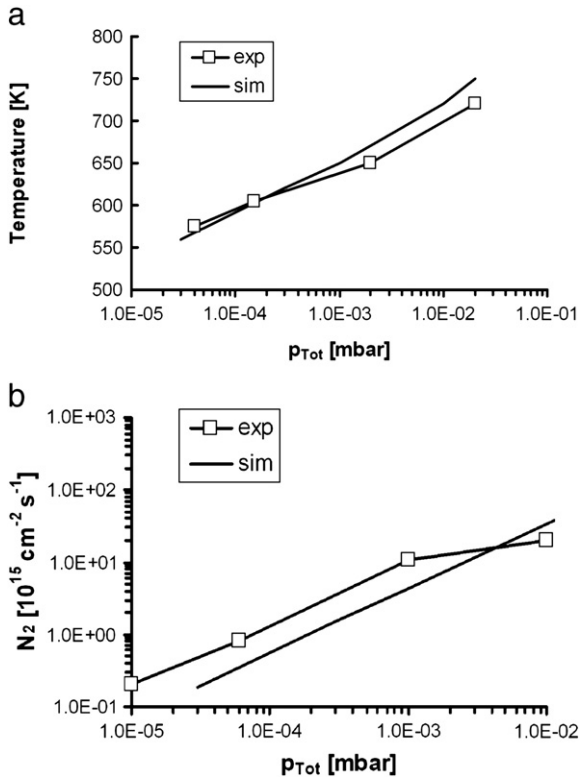

Fig. 4. a) Dependence of the temperature for maximum N_2 production on the total pressure for fixed $p_{O2} : p_{NH3} = 1 : 1$ ratio of the reactants. b) Dependence of the maximum N_2 production rate on the total pressure, same conditions. The experimental data were taken from ref [27,26].

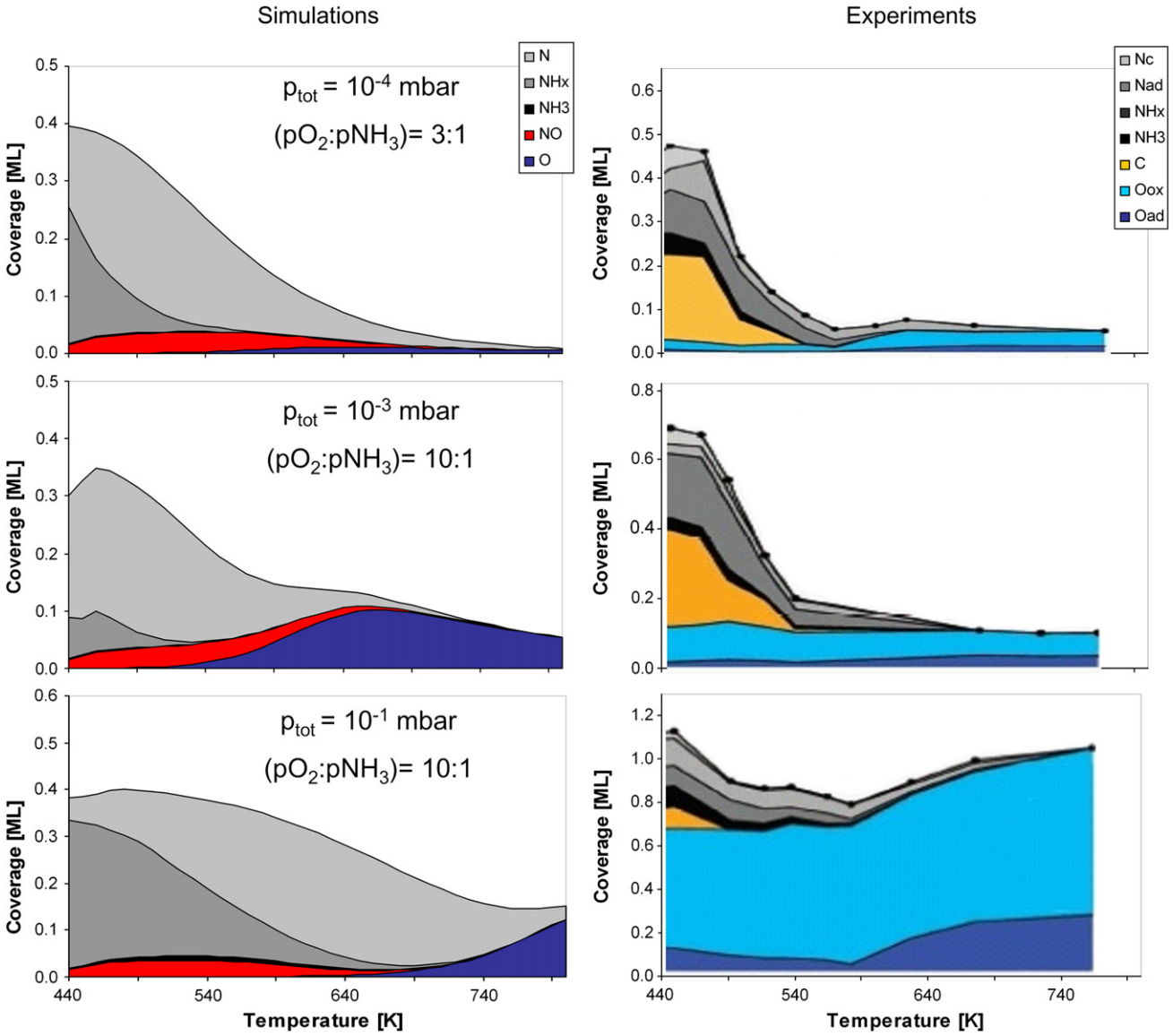

Fig. 5. Temperature profiles of the adsorbate coverages during ammonia oxidation on Pt (533). Comparison between simulated (left column) and experimental adsorbate coverages (right column) for O, NO, NH_3 and NHx (x = 1; 2). The experimental data are from in situ XPS measurements conducted with a Pt (533) sample at low pressure, at 10^{-4} mbar, and at high pressure, at 10^{-1} mbar. The data were taken during heating up the sample with p_{O2} : p_{NH3} ratios of 3 : 1 (top), and 10 : 1 (middle) in the 10^{-4} mbar range; and 10 : 1 (bottom) in the 10^{-1} mbar range. The species O_{OX}, C, and N_C are due to contaminations (s. text). Reaction conditions as follows; top: $p_{O2} = 3\times10^{-4}$ mbar, middle: $p_{O2} = 1\times10^{-3}$ mbar, and bottom: $p_{O2} = 5.5\times10^{-1}$ mbar. Experimental data from ref. [17].

the relative yield increases with rising total pressure is reproduced, as demonstrated in Fig. 6 a–b. Nevertheless, the yield of N_2O we obtain for the 10^{-1} mbar pressure range is still less than 1% of N_2 production. This is by a factor of ≈5 less than the experiments on Pt foil by Baerns et al. [16,18].

From the kinetic parameters calculated for Pt (111), OH adspecies rather than O should promote NH_3 decomposition. In the simulation, the OH-route was observed to play a negligible role, which is simply a consequence of the very low OH coverage (see Fig. 6 b)). The OH species is highly reactive since it can react with NHx (x = 1–3) or disproportionate to form water (step R9). As a very reactive intermediate, the OH concentration remains very low.

As demonstrated by Fig. 9 a) and b), the activation barrier E_5 for the initial step of the O-activated NH_3 decomposition, has a rather strong influence on the catalytic activity and selectivity. Decreasing E_5 by 25% shifts the range of NO production to higher temperature, while simultaneously; the range for N_2 formation is expanded. The activation barriers for the subsequent NH_3 decomposition steps, E_7 and E_9, control the concentration of the intermediates NH and NH_2. As noted above, using an increased barrier of 131 kJ mol^{-1} for E_9 (as originally calculated via DFT for Pt (111)) led to a poisoning of the surface by NH species. Replacing this barrier by the 52 kJ mol^{-1} obtained from a DFT study of Pt (211) also did not lead to reasonable results because then the concentrations of the NHx (x = 1, 2) intermediates became vanishingly small. For this reason E_9 had to be treated as a fit parameter, yielding a value of 84 kJ mol^{-1}.

The second group of kinetic parameters which sensitively influence the catalytic properties are the NO related constants; namely NO formation (step R11), NO decomposition (step $R11^{-1}$), and NO desorption (step R12). As shown in Fig. 7 c), decreasing the activation energy for the N + O recombination step R11 by 25% causes a drastic shrinking of the N_2 production rate, replacing N_2 by NO formation whose onset shifts by roughly 100 K to lower temperature. The opposite effect is seen when the NO desorption energy, E_{18}, is increased by 25%. This suppresses NO formation below 1000 K directing the reaction towards N_2 formation, as can be observed in Fig. 7 d).

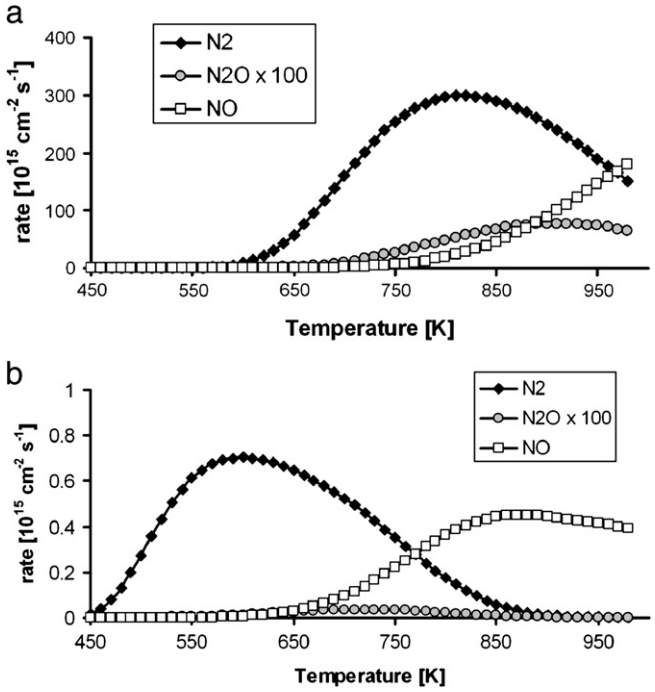

Fig. 6. Simulated N_2O production at low and high pressure with constant $p_{O2} : p_{NH3} = 1 : 1$ ratio of the reactants. Total pressures, (a) $p_{tot} = 1 \times 10^{-1}$ mbar, (b) $p_{tot} = 1 \times 10^{-4}$ mbar.

4. Conclusions

The results in this study have shown that modeling based on the mechanism of oxygen-activated ammonia decomposition allows a very good semiquantitative description of the experimental data. The comparison between experimentally measured and simulated adsorbate coverages also clearly demonstrates that while qualitatively correct behaviour is obtained, quantitative agreement is difficult to achieve. Namely, trends obtained experimentally for TPD and kinetic measurements were successfully reproduced with the proposed model. Regarding surface coverages, a simulation result reflects correctly θ_O coverage variation and its relation with T-range for N_2 or NO preferential product formation.

However, the concept of simply using the kinetic parameters from DFT calculations is only of limited value if one aims at quantitative agreement. The often cited *chemical accuracy* is certainly good enough to discriminate realistic pathways against unrealistic pathways, and thus highly valuable. Quantitative agreement cannot be expected for several reasons which lie in limitations of the mean field approach applied here and in limitations of DFT calculations:

- Energetic interactions decisively influence the kinetic parameters since they increase/decrease activation barriers depending on the coverage and the chemical environment of the reacting species. These dependencies which become very important at high coverage/high pressure are typically neglected in DFT calculations.
- On stepped surfaces which are usually the ones which are important in catalysis only a small subset of all possible reaction pathways can be treated in DFT calculations due to computational limitations. One relies on chemical intuition for the choice of possible pathways, which might be misleading.
- Re structuring effects of the substrate have so far not been considered in DFT calculations. Since the restructuring often creates rough surfaces with structural defects which are known to be very reactive neglecting such effects could mean neglecting the catalytically most active sites.

From the experimental side, most investigations aimed at clarifying basic mechanistic aspects while very basic and simple adsorption studies are left out. These basic studies are however important for quantitative modeling they comprise the influence of coadsorbates on the adsorption kinetics, saturation and inhibition coverages, the formation of coadsorption phases, etc.

The constants which we use in the model are effective constants because the catalytic behaviour of the (111) terraces and (100) steps will be different. Whether the adsorbates on steps and terraces can be considered to be well mixed will depend on the mobility of the adsorbates and on the coverages which may restrict mobility. Depending on pressure and temperature therefore quite different situations might result. For analyzing such situations instead of mean field equations which assume spatial homogeneity lattice gas models would be more appropriate. In particular, at high coverages assuming simple Langmuirian

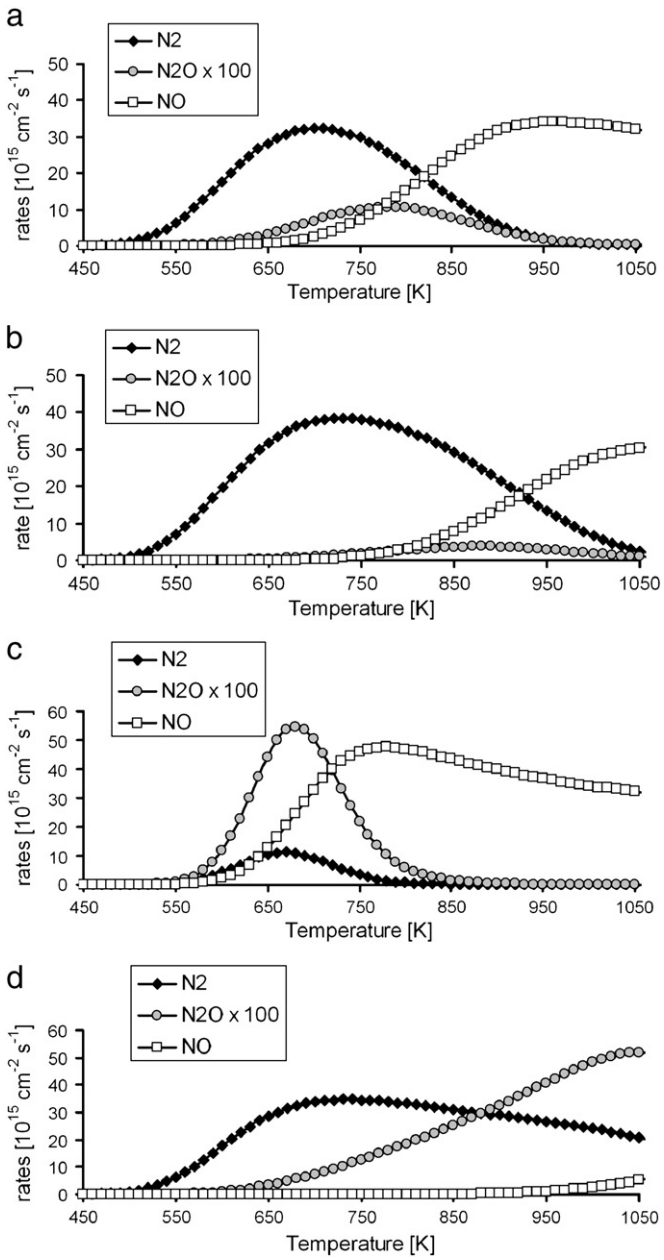

Fig. 7. Sensitivity of the reaction system to the choice of the reaction constants. Shown are temperature profiles of the N2, NO, and N2O production for $p_{O2} : p_{NH3} = 3 : 1$ ratio of the reactants and $p_{O2} = 5 \times 10^{-3}$ mbar. (a) with original values for the constants (b) with E_5 the activation energy for step R3, decreased by 25%, (c) with E_{16}, the activation energy for NO formation (step R11), decreased by 25%, and (d) with E_{18}, the activation energy for NO desorption (step R12), increased by 25%.

adsorption kinetics will be in many cases a rather poor approximation. Attempts in this direction taking into account the different reactivity of local configurations have been made, for example, with catalytic CO oxidation over Ru(0001) [49,50]. Lattice gas models however, typically suffer from the fact that they have to use unrealistically low diffusion jump rates in order to keep simulation tractable.

Instead of attacking the problem from a fundamental level, with a more pragmatic approach one could try to parameterize these dependencies in an ODE model by introducing coverage-dependent constants. This, however, would introduce a number of fit parameters. In the best case, one could hope in succeeding to express very complicated dependencies with a small number of effective parameters.

Summarizing, simulations for ammonia oxidation over a Pt (533) surface were carried using a mean field model which is based on oxygen-activated NH_3 decomposition. The model includes the decomposition intermediates NH and NH_2. Qualitatively, the experimental data are reproduced correctly reaching overall semiquantitative agreement with the experiment. Moreover, the model hereby presented can be used to assess the relative importance of individual steps in the reaction mechanism. Even when the simulations capture a great deal of important experimental features, quantitative agreement is not to be expected due to several limitations inherent to the method; e.g., the use of mean-field equations for a system which is heterogeneous on a microscale and exhibits strong energetic interactions of the adparticles, and neglecting island formation and coverage dependence of kinetic constants.

Acknowledgments

This work was supported by the DFG under the priority program No. 1091 “Bridging the gap between ideal and real systems in heterogeneous catalysis”. M.R., J.L.V., and A.A. gratefully acknowledge financial support from the UNLP (Universidad Nacional de La Plata), CICPBA (Comisión de Investigaciones Científicas de la Prov. de Buenos Aires — Argentina), CONICET (Consejo de Investigaciones Científicas y Tecnológicas), and DAAD (Deutscher Akademischer Austauch Dienst). One of the authors (R.I.) is greatly indebted to W. Offermans for many fruitful discussions. (This work was partially carried while one of the authors (M.R.) was visiting Prof. Imbihl group at Liebniz Hannover University, the kind hospitality and stimulating discussions are gratefully acknowledged).

References

[1] T.H. Chilton, The manufacture of nitric acid by the oxidation of ammonia, Chemical Engineering Progress Monograph Series, 3, American Institute of Chemical Engineers, New York, 1960.
[2] A. Scheibe, M. Hinz, R. Imbihl, Surf. Sci. 576 (1–3) (2005) 131.
[3] G. Novell-Leruth, J.M. Ricart, J. Pérez-Ramírez, J. Phys. Chem. C 112 (2008) 13554.
[4] R. Burch, J. Chem. Phys. 121 (6) (2004) 2737.
[5] R. Burch, J. Chem. Phys. 117 (6) (2002) 2902.
[6] M. Rafti, F. Lovis, Y.F. Zeng, R. Imbihl, Chem. Phys. Lett. 446 (2007) 323.
[7] R. Imbihl, A. Scheibe, Y.F. Zeng, S. Günther, R. Kraehnert, V.A. Kondratenko, M. Baerns, W.K. Offermans, A.P.J. Jansen, R.A. van Santen, Phys. Chem. Chem. Phys. 9 (2007) 3522.
[8] M. Kim, S.J. Pratt, D.A. King, J. Am. Chem. Soc. 122 (2000) 2409.
[9] J.M. Bradley, A. Hopkinson, D.A. King, J. Phys. Chem. 99 (1995) 17032.
[10] J.L. Gland, V.N. Korchak, J. Catal. 53 (1978) 9.
[11] R.W. McCabe, T. Pignet, L.D. Schmidt, J. Catal. 32 (1) (1974) 114.
[12] M. Asscher, W.L. Guthrie, T.H. Lin, G.A. Somorjai, J. Phys. Chem. 88 (1984) 3233.
[13] W.L. Guthrie, J.D. Sokol, G.A. Somorjai, Surf. Sci. 109 (2) (1981) 390.
[14] W.D. Mieher, W. Ho, Surf. Sci. 322 (1995) 151.
[15] D.G. Löfler, L.D. Schmidt, Surf. Sci. 59 (1) (1976) 195.
[16] M. Baerns, R. Imbihl, R. Kraehnert, V.A. Kondratenko, W.K. O-ermans, R.A. van Santen, A. Scheibe, J. Catal. 232 (2005) 226.
[17] S. Günther, A. Scheibe, H. Bluhm, M. Haevecker, E. Kleimenov, A. Knop-Gericke, R. Schlögl, R. Imbihl, J. Phys. Chem. C 112 (2008) 15382.
[18] R. Kraehnert, M. Baerns, Chem. Eng. J. 137 (2008) 361.
[19] W.K. Offermans, A.P.J. Jansen, R.A. van Santen, G. Novell-Leruth, J.M. Ricart, J. Pérez-Ramírez, J. Phys. Chem. C 111 (2007) 17551.
[20] W.K. Offermans, A.P.J. Jansen, R.A. van Santen, Surf. Sci. 600 (2006) 1714.
[21] J.M. Bradley, A. Hopkinson, D.A. King, Surf. Sci. 371 (1997) 255.
[22] A. Scheibe, S. Günther, R. Imbihl, Catal. Lett. 86 (1–3) (2003) 33.
[23] J.M. Gohndrone, C.W. Olsen, A.L. Backman, T.R. Gow, E. Yagasaki, R.I. Masel, J. Vac. Sci. Technol. A 7 (3) (1989) 1986.
[24] E.V. Rebrov, M.H.J.M. de Croon, J.C. Schouten, Development of the kinetic model of platinum catalyzed ammonia oxidation in a microreactor, Chem. Eng. J. 90 (1–2) (2002) 61.
[25] E.V. Rebrov, M.H.J.M. de Croon, J.C. Schouten, A kinetic study of ammonia oxidation on a pt catalyst in the explosive region in a microstructured reactor/heat-exchanger, Chem. Eng. Res. Des. 81 (7) (2003) 744.
[26] A. Scheibe, U. Lins, R. Imbihl, Surf. Sci. 577 (1) (2005) 1.
[27] Y.F. Zeng, R. Imbihl, J. Catal. 261 (2009) 129.
[28] K. Griffiths, T.E. Jackman, J.A. Davies, P.R. Norton, Surf. Sci. 138 (1984) 113.
[29] X.C. Guo, J.M. Bradley, A. Hopkinson, D.A. King, Surf. Sci. 310 (1994) 163.
[30] J.M. Bradley, X.C. Guo, A. Hopkinson, D.A. King, J. Chem. Phys. 104 (11) (1996) 4283.
[31] L. Vattuone, L. Savio, M. Rocca, Surf. Sci. Rep. 63 (3) (2008) 101.
[32] M. Flytzani-Stephanopoulos, L.D. Schmidt, Prog. Surf. Sci. 9 (3) (1979) 83.
[33] J.M. Gohndrone, R.I. Masel, Surf. Sci. 209 (1–2) (1989) 44.
[34] J.M. Gohndrone, Y.O. Park, R.I. Masel, Surf. Sci. 95 (1) (1985) 244.
[35] R.J. Gorte, L.D. Schmidt, J.L. Gland, Surf. Sci. 109 (2) (1981) 367.
[36] T. Sugisawa, J. Shiraishi, D. Machihara, K. Irokawa, H. Miki, C. Kodama, T. Kuriyama, T. Kubo, H. Nozoye, Appl. Surf. Sci. 169–170 (2001) 292.
[37] M. Rafti, J.L. Vicente, H. Uecker, R. Imbihl, Chem. Phys. Lett. 421 (4–6) (2006) 577,583.
[38] A. Rar, T. Matsushima, Surf. Sci. 318 (1–2) (1994) 89.
[39] A.T. Gee, B.E. Hayden, J. Chem. Phys. 113 (2000) 10333.
[40] G.B. Fischer, Chem. Phys. Lett. 79 (3) (1981) 452.
[41] S.J. Lombardo, T. Fink, R. Imbihl, J. Chem. Phys. 98 (7) (1993) 5526.
[42] A.B. Anton, D.C. Cadogan, Surf. Sci. Lett. 239 (1990) L548.
[43] V.I. Savchenko, N.I. Efremova, React. Kinet. Catal. Lett. 56 (1) (1995) 97.
[44] E.H.G. Backus, A. Eichler, M.L. Grecea, A.W. Kleyn, M. Bonn, J. Chem. Phys. 121 (16) (2004) 7946.
[45] A. Bogicevic, K.C. Hass, Surf. Sci. Lett. 506 (2002) L237.
[46] Q. Ge, M. Neurock, J. Am. Chem. Soc. 126 (5) (2004) 1551.
[47] S. Völkening, K. Bedürftig, K. Jacobi, J. Wintterlin, G. Ertl, Phys. Rev. Lett. 83 (1999) 2672.
[48] A. Michaelides, P. Hu, J. Chem. Phys. 114 (2001) 513.
[49] B. Temel, K. Reuter, Phys. Rev. B 73 (2006) 045433.
[50] K. Reuter, H. Meskine, M. Schefler, H. Metiu, J. Chem. Phys. 126 (2007) 204711.